Molecular Therapy
Methods & Clinical Development
Original Article

Ex Vivo Cell Therapy by Ectopic Hepatocyte Transplantation Treats the Porcine Tyrosinemia Model of Acute Liver Failure

Clara T. Nicolas,[1,2,3] Robert A. Kaiser,[1,6] Raymond D. Hickey,[4] Kari L. Allen,[1] Zeji Du,[1] Caitlin J. VanLith,[1] Rebekah M. Guthman,[1,5] Bruce Amiot,[1] Lukkana Suksanpaisan,[7] Bing Han,[8] Maria Giovanna Francipane,[8,9] Amin Cheikhi,[10] Huailei Jiang,[11] Aditya Bansal,[11] Mukesh K. Pandey,[11] Ishan Garg,[11] Val Lowe,[11] Aditya Bhagwate,[12] Daniel O'Brien,[12] Jean-Pierre A. Kocher,[12] Timothy R. DeGrado,[11] Scott L. Nyberg,[1] Eric Lagasse,[8,14] and Joseph B. Lillegard[1,6,13,14]

[1]Department of Surgery, Mayo Clinic, Rochester, MN 55905, USA; [2]Faculty of Medicine, University of Barcelona, Barcelona, Spain; [3]Department of Surgery, University of Alabama Birmingham, Birmingham, AL, USA; [4]Ambys Medicines, San Francisco, CA, USA; [5]Medical College of Wisconsin, Wausau, WI, USA; [6]Children's Hospitals and Clinics of Minnesota, Midwest Fetal Care Center, Minneapolis, MN, USA; [7]Imanis Life Sciences, Rochester, MN, USA; [8]McGowan Institute for Regenerative Medicine and Department of Pathology, University of Pittsburgh, Pittsburgh, PA, USA; [9]Ri.MED Foundation, Palermo, Italy; [10]Department of Physical Medicine and Rehabilitation, University of Pittsburgh, Pittsburgh, PA, USA; [11]Department of Radiology, Mayo Clinic, Rochester, MN, USA; [12]Department of Biomedical Statistics and Informatics, Mayo Clinic, Rochester, MN, USA; [13]Pediatric Surgical Associates, Minneapolis, MN, USA

The effectiveness of cell-based therapies to treat liver failure is often limited by the diseased liver environment. Here, we provide preclinical proof of concept for hepatocyte transplantation into lymph nodes as a cure for liver failure in a large-animal model with hereditary tyrosinemia type 1 (HT1), a metabolic liver disease caused by deficiency of fumarylacetoacetate hydrolase (FAH) enzyme. Autologous porcine hepatocytes were transduced *ex vivo* with a lentiviral vector carrying the pig *Fah* gene and transplanted into mesenteric lymph nodes. Hepatocytes showed early (6 h) and durable (8 months) engraftment in lymph nodes, with reproduction of vascular and hepatic microarchitecture. Subsequently, hepatocytes migrated to and repopulated the native diseased liver. The corrected cells generated sufficient liver mass to clinically ameliorate the acute liver failure and HT1 disease as early as 97 days post-transplantation. Integration site analysis defined the corrected hepatocytes in the liver as a subpopulation of hepatocytes from lymph nodes, indicating that the lymph nodes served as a source for healthy hepatocytes to repopulate a diseased liver. Therefore, ectopic transplantation of healthy hepatocytes cures this pig model of liver failure and presents a promising approach for the development of cures for liver disease in patients.

INTRODUCTION

Nearly 14,000 patients wait annually for liver transplantation in the United States. The problem is considerably worse world-wide and represents one of the most challenging hurdles in medicine.[1] With a universal shortage of organs and limited resources, alternatives to whole organ transplantation are required to address this problem. Bioartificial liver devices and repopulation of decellularized liver scaffolds for transplantation have yet to prove effective as treatments for liver failure. Cell therapy using primary hepatocytes has shown effectiveness in animal models, but the success of this approach has been limited in the clinical setting,[2] often due to the inflammation, fibrosis, and scar tissue in the failing liver, creating an adverse environment for hepatocyte engraftment and growth.[3]

Hereditary tyrosinemia type 1 (HT1) is an ideal disease model to study treatment options for acute and chronic liver failure. HT1 is an inborn error of metabolism of the liver caused by a deficiency of the fumarylacetoacetate hydrolase (FAH) enzyme, which is responsible for the last step of tyrosine catabolism.[4] Untreated, HT1 rapidly produces inflammatory changes and liver injury, often leading to fulminant liver failure as early as a few months of life.[5] In the chronic form, HT1 leads to persistent accumulation of toxic metabolites in hepatocytes, causing oxidative damage and subsequent inflammation, fibrosis, cirrhosis, and high rates of hepatocellular carcinoma (HCC).[6,7] HT1 is clinically managed using 2-(2-nitro-4-trifluoromethylbenzoyl)-1,3-cyclohexanedione (NTBC), a drug that inhibits tyrosine metabolism upstream of FAH, leading to the build-up of less toxic metabolites.[8] However, there is no true cure for HT1 short of liver transplantation.

We have previously created and characterized the porcine model of HT1 and showed that this animal is an excellent model of acute

Received 18 February 2020; accepted 7 July 2020;
https://doi.org/10.1016/j.omtm.2020.07.009.

[14]These authors contributed equally to this work.

Correspondence: Joseph B. Lillegard, Department of Surgery, Mayo Clinic, 200 First Street SW, Rochester, MN 55905, USA.
E-mail: jlillegard@msn.com

and chronic liver failure by reproducing the inflammation, fibrosis, and cirrhosis pattern seen in many human liver diseases.[9] We have since demonstrated that *ex vivo* gene therapy involving lentiviral transfer of a functional *FAH* cDNA into autologous hepatocytes is curative in mouse and pig models of HT1.[10] In our previous work, primary hepatocytes for correction were isolated from a partial hepatectomy, and corrected cells were transplanted back into donor animals via portal vein infusion. However, orthotopic hepatocyte transplantation may not be feasible in all patients with liver disease, as the diseased liver is often an inadequate and hostile environment for transplanted hepatocytes.[11]

Ectopic sites for transplantation could provide a healthy milieu to enable hepatocyte engraftment. Lymph nodes are a readily accessible alternative due to several defining characteristics. For example, they are prepared to harbor rapid expansion of T and B cells to support a swift immune response when needed,[12,13] and they provide a favorable environment for metastatic cell engraftment and growth.[14] This is due, in part, to their high vascularization potential, which permits neoangiogenesis,[15,16] as well as to their reticular network of fibroblasts and other stromal cells that provide physical and trophic support.[17,18] Lastly, inherent plasticity and continued functionality, despite accommodation of immigrant cells, make lymph nodes a promising site for ectopic cell delivery.[19] Indeed, intraperitoneal transplantation of hepatocytes in mice results in colonization of lymph nodes and rescue from lethal hepatic failure.[20]

We explored the mouse lymph node as an ectopic transplantation site for multiple tissues, including liver, and demonstrated that injection of hepatocytes into a single lymph node generated enough ectopic liver mass to rescue the metabolic disorder in the mouse model of HT1.[21] In the current study, we demonstrate the therapeutic potential of ectopic transplantation of *ex vivo*-corrected hepatocytes into lymph nodes in a large animal model of liver failure, the HT1 pig, and show long-term engraftment in the mesenteric lymph nodes, resulting in generation of important liver architecture and serving as a reservoir for repopulation of the recovering native liver, with multiple cell lineages seen in the native liver.

RESULTS

Hepatocytes Engraft in Mesenteric Lymph Nodes after Ectopic Transplantation

A wild-type pig underwent a partial hepatectomy, and harvested hepatocytes were labeled with ^{89}Zr (half-life [$t_{1/2}$] 78.4 h)[22] prior to transplantation into 10–20 mesenteric lymph nodes. Radiolabeling efficiency was ~20%, and radioactivity concentration was ~0.1 MBq/10^6 cells. The animal received 6×10^8 hepatocytes through direct mesenteric lymph node injection. Positron emission tomography-computed tomography (PET-CT) imaging at 6, 54, and 150 h post-transplantation demonstrated the presence of radioactivity within mesenteric lymph nodes (261.8 ± 108.7, 101.1 ± 34.7, and 70.0 ± 26.4 standardized uptake value [SUV], respectively; Figure 1D; Video S1) with background activity measuring (0.1 SUV) in the lumbar paraspinal muscles. Interestingly, although no radioactivity was detected within the liver at the 6-h time point, increasing levels were in the liver at the 54- and 150-h time points (3.3 ± 0.4 and 5.9 ± 0.8 SUV, respectively), indicating accumulation of ^{89}Zr-labeled cells or cellular debris. The absence of radioactivity in bone, a known site of uptake for unchelated ^{89}Zr, suggested that the radiolabel was retained within the dinitrobenzamide (DBN) chelator construct and not indicative of an unincorporated "free" label. These data at 0.69 and 1.9 $t_{1/2}$, respectively, suggest possible migration of the transplanted hepatocytes from the lymph nodes to the liver or labeled cellular debris passing through the liver. No radioactivity above background was found in the spleen, lung, or other organ systems at either of these time points.

Ex Vivo-Corrected Hepatocytes Are Able to Cure a Pig Model of Acute Liver Failure after Ectopic Transplantation into Lymph Nodes

A total of 5, 8-week-old $Fah^{-/-}$ animals were maintained on NTBC until the time of *ex vivo*-corrected autologous hepatocyte transplantation into lymph nodes (Figures 1A–1C). Each animal was anesthetized, and a laparoscopic partial hepatectomy was conducted to provide the cells for *ex vivo* gene therapy. Isolated hepatocytes were transduced with lentiviral vectors expressing the *Fah* or sodium/iodide symporter (*Nis*) transgenes, both under the control of the hepatocyte-specific thyroxine-binding globulin (TBG) promoter. After transduction, the modified autologous hepatocytes were transplanted into multiple mesenteric lymph nodes. All animals were autotransplanted with a total of 6×10^8 *ex vivo*-transduced hepatocytes from individual preparations at 74%–85% post-isolation viability for doses of 2.9–3.7 $\times$ 10^7 total cells per kilogram (Table S1; Figure S1). This is an order of magnitude less than the total number of cells transplanted in several reports of humans with metabolic liver disease, most of which received liver transplants a few months later.[23] NTBC administration was discontinued to propagate liver failure and provide the regenerative stimulus for selective healthy hepatocyte expansion. Animals were cycled on and off NTBC, based on weight parameters, until NTBC-independent growth was achieved (Figures 2A and S2), occurring at a mean of 135 ± 25 days post-transplantation (range: 97 to 161 days) after 3 to 6 cycles of NTBC.

Biochemical cure of the proceeding liver failure and HT1 phenotype was confirmed by normalization of liver-specific enzymes and tyrosine levels. At the time of euthanasia, mean (±standard deviation) tyrosine levels for the five animals were (84.2 ± 34.5 μM), which was within wild-type range and was significantly lower than untreated $Fah^{-/-}$ controls (826.3 ± 277.5 μM) (Figure 2B). Similar results were seen in mean (±standard deviation) liver-function tests in treated animals (aspartate aminotransferase [AST]: 56.8 ± 21.7 U/L, alkaline phosphatase [ALP]: 186.6 ± 78.8 IU/L, ammonia: 35.8 ± 14.4 μM, albumin: 3.6 ± 0.3 g/dL, and total bilirubin: 0.15 ± 0.1 mg/dL) compared to untreated $Fah^{-/-}$ controls (AST: 343.7 ± 54.5 U/L, ALP: 918.3 ± 282.5 IU/L, ammonia: 553 ± 561.3 μM, albumin: 2.8 ± 0.9 g/dL, and total bilirubin: 1 ± 0.7 mg/dL).

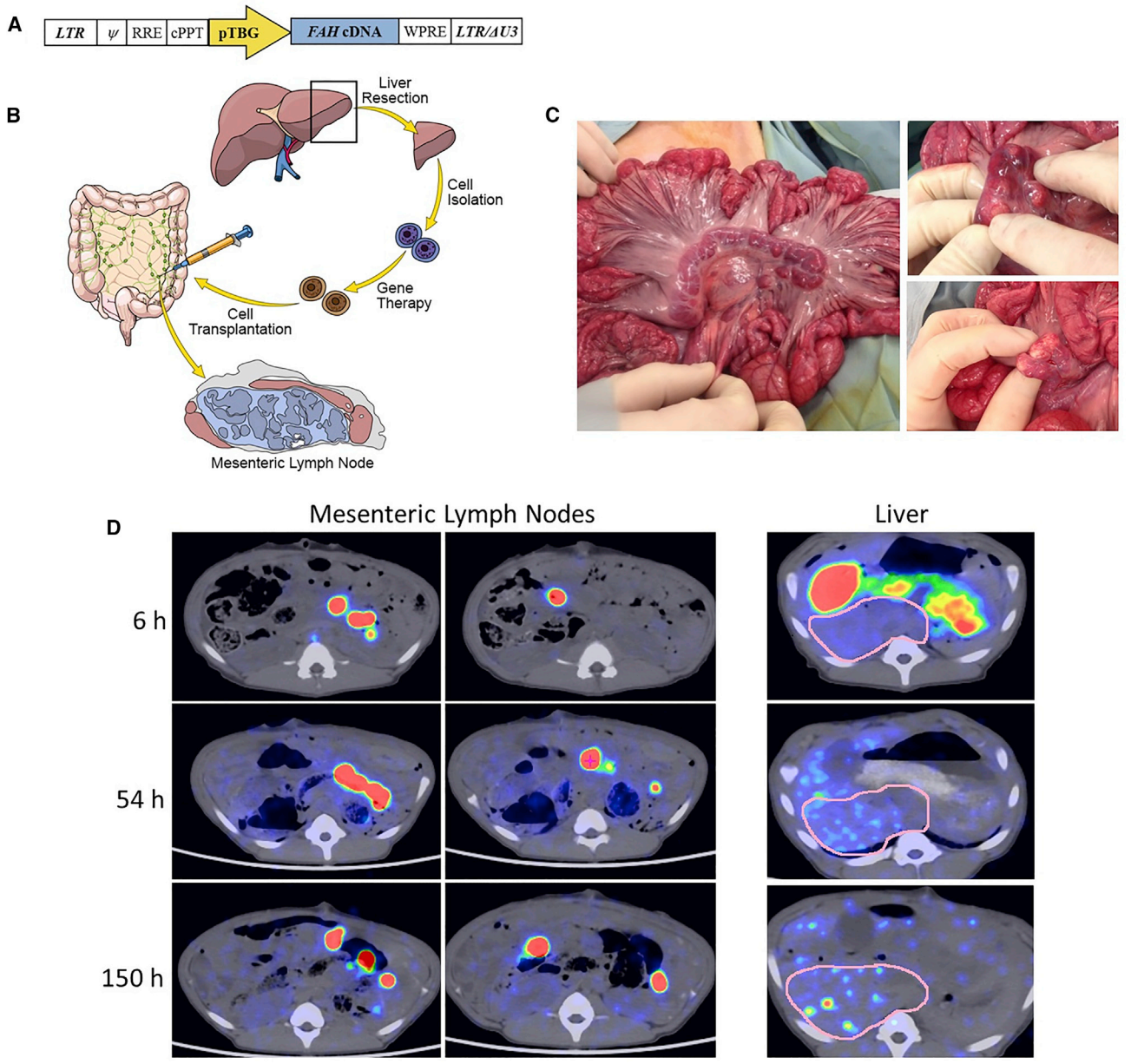

Figure 1. Schematic of the Lentiviral Vector and Experimental Process and PET-CT Images of Transplanted ^{89}Zr-Labeled Hepatocytes

(A) The human *FAH* cDNA is under control of the pig thyroxine-binding globulin (pTBG) promoter. LTR, long terminal repeat; Ψ, psi packaging sequence; RRE, Rev-responsive element; cPPT, central polypurine tract; LTR/ΔU3, 3′ long terminal repeat with deletion in U3 region. (B) Four steps are involved in this process: (1) partial hepatectomy, (2) primary hepatocyte isolation, (3) *ex vivo* gene delivery, and (4) autotransplantation of hepatocytes into mesenteric lymph nodes. (C) Macroscopic appearance of the mesenteric lymph nodes before (left) and after (right) hepatocyte transplantation. (D) Representative axial images showing the presence of ^{89}Zr-labeled hepatocytes in the mesenteric lymph nodes within 6 h of transplantation in a single pig and engraftment maintained at nearly 1 week post-transplantation. At the 54 and 150 h time points, hepatocyte engraftment is observed within the liver, as well as in the mesenteric lymph nodes. Regions of interest in the liver (pink outlines) show no positive hepatocytes at 6 h and multifocal positivity at 54 and 150 h.

Hepatocytes Transplanted into Lymph Nodes Demonstrate Long-Term Survival

We performed PET/CT imaging of 2 pigs (numbers 265 and 268) that were cotransduced with separate lentiviral vectors carrying the *Fah* and *Nis* transgenes to monitor for the expansion/distribution of NIS-positive hepatocytes. Prior to imaging, animals received 10 mCi (370 MBq) of [^{18}F]tetrafluoroborate ([^{18}F]TFB). Pig number 265 was scanned at 104 and 203 days, and pig number 268 was

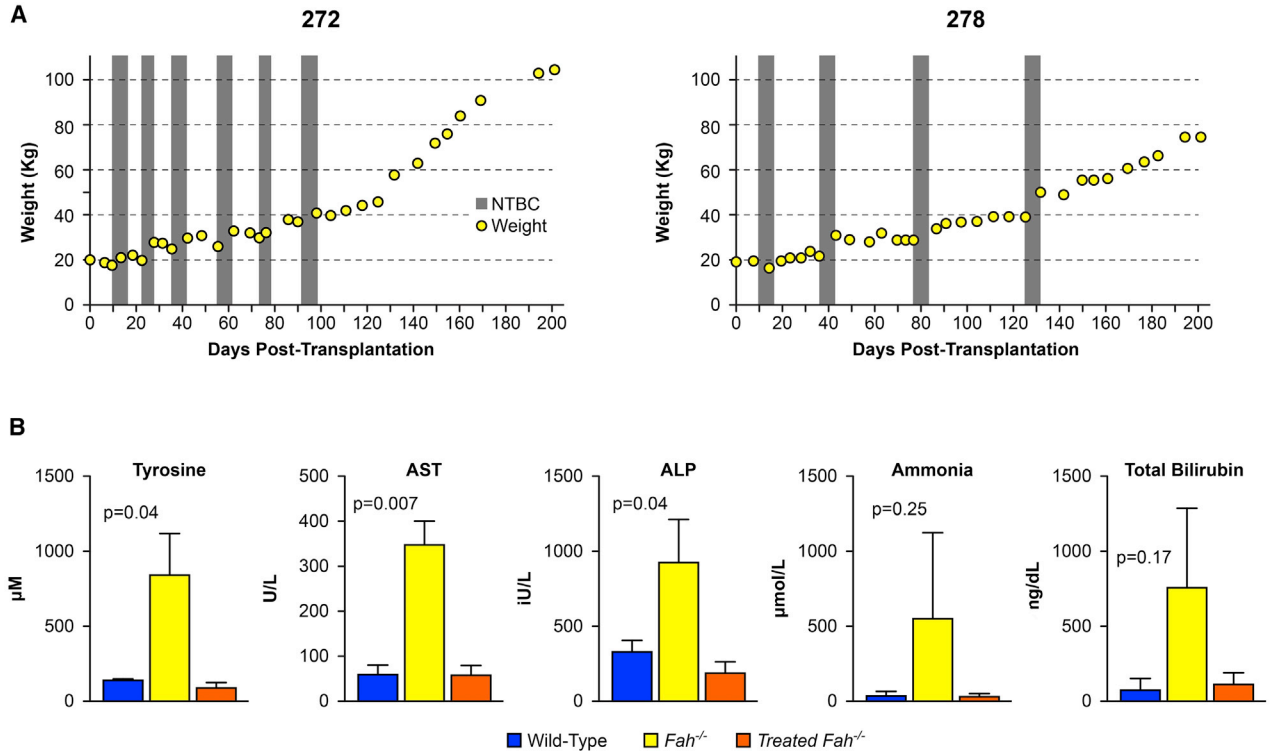

Figure 2. Weight Gain and Biochemical Correction of Treated Pigs

(A) Weight stabilization of pigs 272 and 278 demonstrating NTBC-independent growth at days 97 and 131 post-transplantation. Periods of NTBC administration are indicated by gray vertical bars. (B) Normalization of tyrosine, aspartate aminotransferase (AST), alkaline phosphatase (ALP), ammonia, and total bilirubin levels at the time of euthanasia in all animals. Mean ± SD is shown for experimental animal cohort (treated $Fah^{-/-}$ animals, n = 5) alongside historical wild-type (n = 4) and untreated $Fah^{-/-}$ (n = 3) control animals. p values are provided for the experimental animal cohort compared to untreated $Fah^{-/-}$ controls.

scanned at 177 and 203 days post-transplantation. Both animals showed NIS positivity in mesenteric lymph nodes (15.7 and 39.0 SUV and 92.6 and 32.0 SUV, respectively; Figure 3A; Videos S2, S3, S4, and S5). Despite greater than 50% repopulation of the liver at necropsy with FAH-positive hepatocytes, minimal NIS activity was seen in the liver, owing to the fact that only a subpopulation of transplanted hepatocytes is doubly transduced, engrafts in the lymph nodes, and then migrates and expands in the liver.

To correlate NIS positivity in mesenteric lymph nodes with histological findings, previously targeted lymph nodes were biopsied at day 140 post-transplantation. All lymph node samples were taken from the root of the mesentery, and over one dozen lymph nodes in each animal were grossly positive for hepatic tissue and later confirmed by immunohistochemistry (IHC) staining for FAH (Figure 3B), which would be unique to the corrected hepatocytes. Amplified regions demonstrate the presence of homogeneous-staining nodules of different intensities, indicative of expansion of multiple distinct hepatocyte founders (Figure 3B, middle). All experimental animals were euthanized at 212 to 241 days post-transplantation. Histology of the collected mesenteric lymph nodes showed a sustained presence of FAH-positive hepatocytes (Figure 3B, right), which was observed in four out of five animals. The two animals that had been biopsied previously still had FAH-positive hepatocyte engraftment in lymph nodes at necropsy, confirmed by FAH and cytokeratin 18 IHC staining (Figure 3B, left and middle). Cluster of differentiation (CD)31-positive endothelial cells were found within areas of hepatocyte engraftment (Figure 3B; pig 268, bottom right), suggesting that significant blood vessel remodeling took place after transplantation to sustain engraftment and growth. Positivity for glutamine synthetase, an enzyme exclusively expressed in pericentral hepatocytes in mammals,[24] was found in hepatocytes surrounding CD31-positive neovessels. This suggests neo-formation of a central vein and importantly, proper physiological zoning of the ectopic liver. Reproduction of hepatic microarchitecture within transplanted lymph nodes was further supported by the presence of hepatic lobules similar to those observed in native pig livers and rare cytokeratin 7-positive bile duct cells (Figure 3B; pig 265, bottom right) and cytokeratin 7 and 19 double-positive cells present at the periphery of some lymph node engraftment sites (Figure S3).

Hepatocyte-Engrafted Lymph Nodes Serve as a Reservoir for Liver Repopulation

The presence of corrected hepatocytes in the liver was revealed by IHC of liver tissue demonstrating multiple FAH-positive nodules within the livers of all five animals, covering 67% to 100% (84.7 ± 7.0)

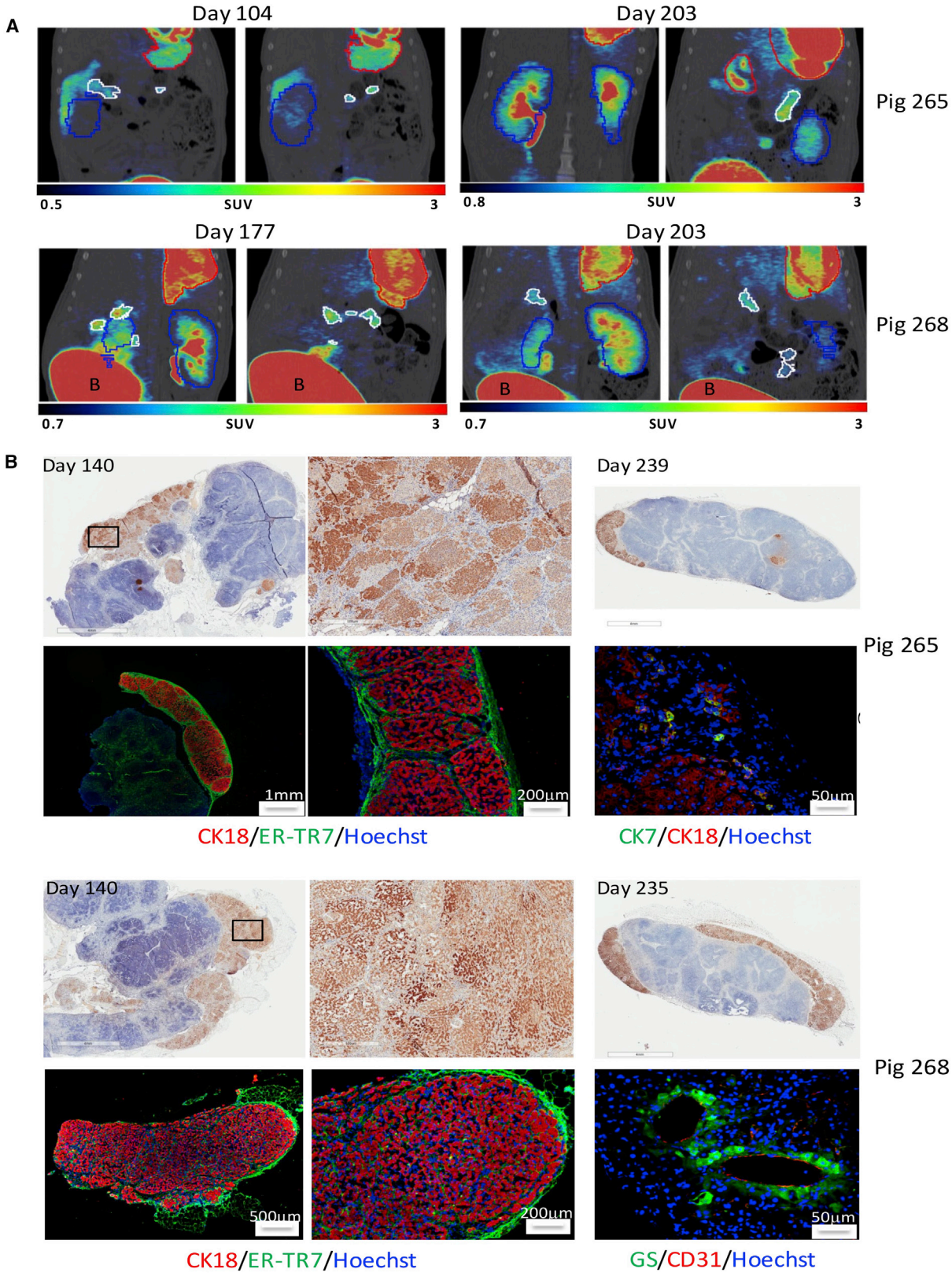

(legend on next page)

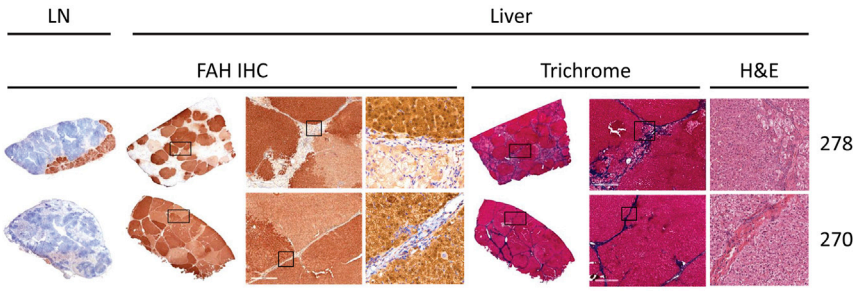

Figure 4. Liver Repopulation with FAH-Positive Hepatocytes

Pig 278: IHC showing the presence of FAH-positive hepatocytes in mesenteric lymph node (left) and liver (center) at day 239 post-transplantation; trichrome (center right) showing hepatocellular damage and fibrosis in FAH-negative areas of the liver at day 239 post-transplantation. H&E (right) showing cellular morphology in corrected and diseased nodules. Pig 270: IHC showing minimal presence of FAH-positive hepatocytes in mesenteric lymph node (left) and complete liver repopulation with FAH-positive cells (center) at day 241 post-transplantation; trichrome (center right) showing resolution of fibrosis with minimal residual scarring in FAH-repopulated livers at day 241 post-transplantation. H&E (right) showing cellular morphology in a uniformly corrected field of liver tissue.

of the total liver area at the time of necropsy. An inverse correlation was found between percent liver repopulation with FAH-positive hepatocytes and a sustained presence of FAH-positive hepatocytes within lymph nodes. Pigs with complete liver repopulation with FAH-positive hepatocytes showed little hepatocyte presence within lymph nodes at termination, whereas pigs with only partial liver repopulation with FAH-positive hepatocytes demonstrated a more robust hepatocyte presence within lymph nodes (Figure S4). As expected, FAH-negative areas of the liver still undergoing repopulation showed hepatocellular damage and fibrosis, whereas the two fully FAH-positive livers demonstrated healthy, normal-looking tissue, suggesting that the severe hepatic injury that occurs while off NTBC is reversible as FAH-positive hepatocytes expand to repopulate the liver (Figure 4). At termination (approximately 8 months), active hepatocyte proliferation was unremarkable in both lymph nodes and livers, as evaluated by Ki-67 staining (Figure S5)

In order to characterize any differences between the hepatocytes present in the liver and those present in the lymph nodes, we performed an in-depth bioinformatics analysis of both populations from a representative animal (pig number 265). Mapping statistics of over 130 million total reads are provided in Table S2. We found no significant differences in a general lentiviral integration profile between these two cell populations. In both cases, integration occurred more often in coding regions than in noncoding regions, with exons preferred over introns (Figure 5A), and integration was favored in chromosomes with higher gene densities (Figure S6B). In both cell populations, lentiviral integration was rare in CpG-rich islands and was clearly favored downstream of transcription start sites (Figures 5B and 5C), suggesting minimal tumorigenicity potential from oncogene activation. Furthermore, there was no preference for integration in tumor-associated genes in either cell population (Figure 5D).

The genes with the highest integration frequency in both groups of cells are presented in Table 1. *Fah* had the highest number of distinct integration sites in both liver and lymph node. However, it was only included in the top ten integrated genes in the lymph node population due to the multiplicity of some specific integration sites in other genes. Interestingly, all but two of the 135 unique integration sites within *Fah* in the liver hepatocytes were represented in the 206 integration sites present in the lymph node hepatocytes (Figure 5E), indicating that the transplanted cells first engrafted in the lymph nodes, divided, and then migrated to the liver. The top four genes with the highest integration frequency in the liver population were also within the top 20 genes in the lymph node population and were all approximately 5-fold enriched in the liver population when evaluated by the total number of reads present for each, suggesting unbiased expansion and enrichment of a subpopulation of lymph node hepatocytes within the liver. These genes were the following: *Mir9799* (microRNA), *Ndufv2* (NADH dehydrogenase ubiquinone flavoprotein 2), *Ifrd1* (interferon-related developmental regulator 1), and *Suclg1* (succinyl-coenzyme A [CoA] ligase (guanosine diphosphate [GDP]-forming), alpha subunit). In native (repopulated) and ectopic liver (hepatized lymph node [HLN]) samples obtained at necropsy, expression of representative genes in this list (*Suclg1*, *Ndufv2*, and *Ifrd1*) was indeed disrupted compared to control liver (CL) levels, which may have been

Figure 3. Long-Term Presence of Ectopic Liver Tissue in Mesenteric Lymph Nodes

(A) PET-CT images of NIS-labeled hepatocytes at 104, 177, and 203 days post-transplantation into mesenteric lymph nodes. Representative coronal images showing persistent engraftment of NIS-labeled hepatocytes in the mesenteric lymph nodes in pigs 265 and 268. Mesenteric lymph nodes are outlined in white, stomach in red, and kidney in blue; bladder, "B." (B) Histological confirmation of ectopic hepatocyte presence in mesenteric lymph nodes at 140 and 235–239 days post-transplantation. Pig 265: IHC showing the presence of FAH-positive hepatocytes at days 140 (top left, middle) and 239 (top right) post-transplantation. Immunofluorescence at day 239 showing cytokeratin 18 (CK18; red)-positive hepatocytes and reticular fibroblasts (ER-TR7; green) on a Hoechst background (bottom left, middle) and cytokeratin 7 (CK7; green)-positive bile-duct cells (bottom right). Pig 268: IHC showing the presence of FAH-positive hepatocytes at days 140 (top left, middle) and 235 (top right) post-transplantation. Immunofluorescence at day 235 showing CK18 (red)-positive hepatocytes and reticular fibroblasts (ER-TR7; green) on a Hoechst background (bottom left, middle) and glutamine synthetase (GS; green)-positive hepatocytes around CD31-positive endothelial cells (red), forming possible central vein (bottom right).

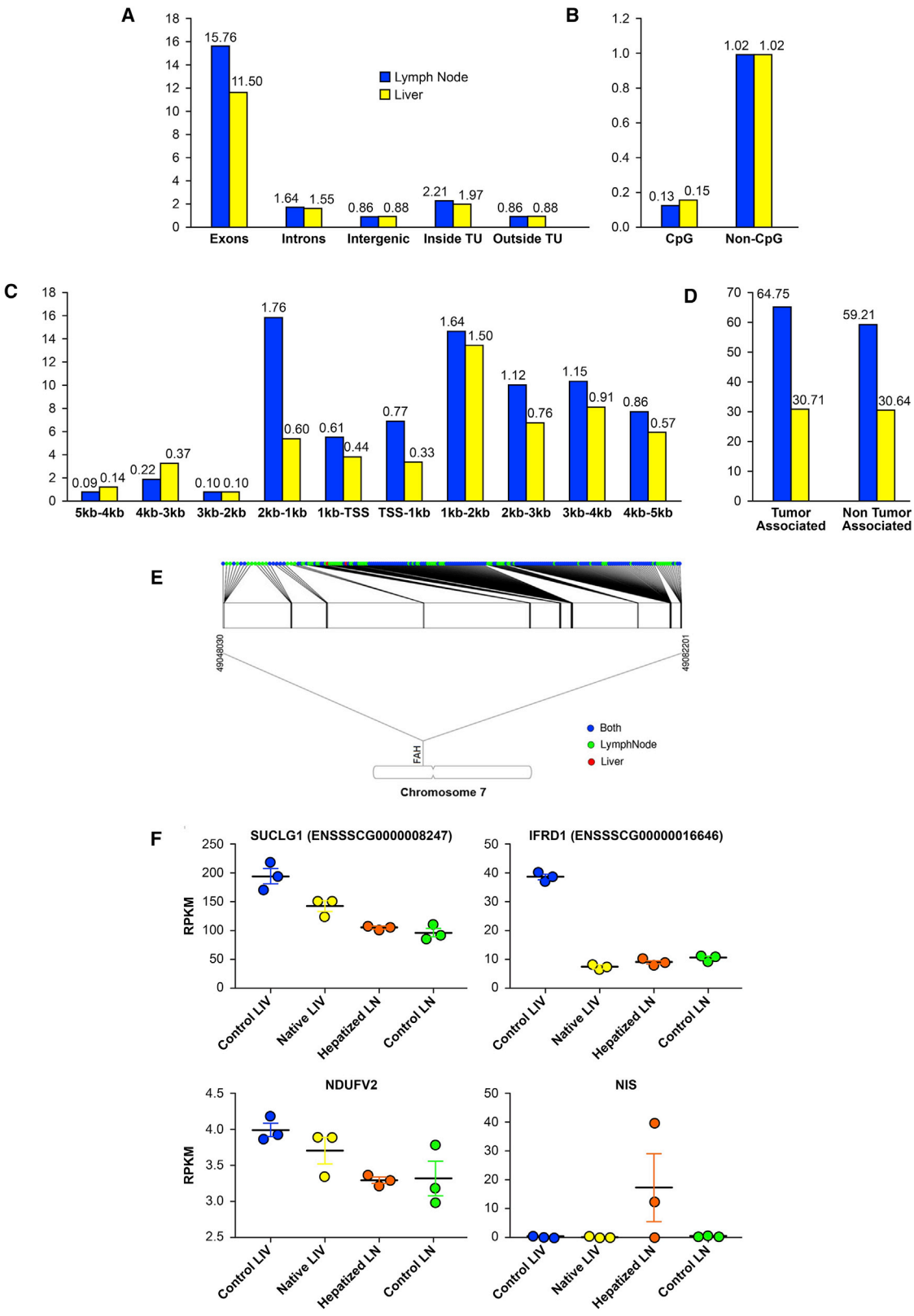

(legend on next page)

due to vector insertion and disruption in at least one allele in some cells (Figure 5F). As a control, NIS expression was evaluated and only detectable in 2 of the 3 samples of HLNs analyzed. The fifth most prevalent integration site in the hepatocytes that migrated to the liver was *Cenpp* (centromere protein P), which was enriched over 78-fold compared to the lymph node population and could be an indication that this disruption strongly favored the migration, engraftment, and/or expansion potential cells harboring this integration.

To determine whether ectopic hepatocytes generated tissue-resembling normal liver, transcriptome profiles of untransplanted control lymph node (CLN) and HLNs, as well as engrafted native liver and untreated CLs, were compared. Twelve-thousand differentially expressed (DE) genes were identified and contrasted to an untreated CLN and CL (Figure 6A). t-Distributed Stochastic Neighbor Embedding (t-SNE) showed a strong tendency of HLN transcripts to cluster with liver tissues samples, especially engrafted native liver (NL), whereas CLNs were distinct from the other groups (Figure 6B). Therefore, a significant proportion of the lymph node transcriptome acquired a liver-like phenotype after hepatocyte transplantation. We analyzed 24 liver-specific gene expression panels (LiGEPs; Table S3; Figure S6) and 20 additional genes (cytochrome P450s, other enzymes, plasma proteins, transporters, surface molecules and cytokines, and transcription factors; Table S3) showing HLN expression of multiple proteins approaching liver values. Indeed, cluster heatmaps show a liver-like expression profile for HLN, indicating substantial hepatocyte phenotype (Figure 6C). Specifically, evaluation of albumin expression demonstrates adoption of a liver phenotype by HLNs relative to control (Figure 6D, left), whereas analysis of *FAH* shows transgenic expression in HLNs, as well as elevated transgenic expression in repopulated native liver relative to control (Figure 6D, right). Expression levels of all other genes are shown in Figures S7A and S7B (LiGEP and additional liver-specific genes, respectively).

DISCUSSION

Ectopic hepatocyte transplantation has been attempted in several preclinical and clinical studies,[19] as orthotopic hepatocyte transplantation is often limited by pre-existing liver injury associated with disease, such as inflammation, fibrosis, and cirrhosis.[11] Of the alternative sites tested, only peritoneal cavity and spleen have been able to accommodate a clinically significant number of cells.[25] Intraperitoneal transplantation of hepatocytes has been attempted in humans with acute liver failure, but transplanted cells are not able to survive in this environment for extended periods.[26] However, intrasplenic injection of hepatocytes improves liver function and prolongs survival in a mouse model of liver failure.[27] Although transplenic access to the portal vein in human patients has been described,[28] this may pose a significant hemorrhagic risk. Lymph nodes are a highly favorable site for ectopic cell transplantation.[19,29–31] Not only do their plasticity and highly complex vascular network provide a healthy milieu for cell engraftment and expansion, but their accessibility makes it possible to perform minimally invasive cell delivery in the clinical setting. Ultrasound-guided lymph node identification and targeting are commonly performed clinically, and multiple clinical studies have employed lymph nodes as sites for injection of immunotherapeutic agents, with patients rating the procedure comparable to a subcutaneous injection and less painful than venipuncture.[32] Furthermore, cell transplantation into lymph nodes does not appear to affect lymph node function in this or previous studies.[20,21]

Hepatocyte transplantation into lymph nodes is able to generate enough ectopic liver mass to correct HT1 and rescue mice from acute and chronic liver disease.[21] However, the HT1 mouse does not exhibit the full extent of liver injury seen in humans, including fibrosis and cirrhosis.[21] We now show a similar result in the large animal model of HT1, suggesting that ectopic hepatocyte transplantation is scalable and may be clinically translatable to metabolic disease-induced liver failure. The current study was conducted in the HT1 pigs initially supported on NTBC, where liver disease could be delayed until the harvesting of autologous cells was complete. However, 1–2 weeks after the withdrawal of NTBC, the porcine model develops rapid and severe liver injury that includes the inflammation, fibrosis, and cirrhosis similar to human liver failure.[9,33] Hepatocyte engraftment and ectopic liver development in lymph nodes of HT1 pigs and mice are driven by native liver injury,[34] a consequence of NTBC removal to establish tyrosinemia. We have shown previously that partial hepatectomy is also able to transiently induce hepatocyte proliferation in lymph nodes due to liver injury,[20,21] but further work is needed to verify if a similar process is possible in human liver diseases outside of HT1 with its natural selective advantage for corrected hepatocytes. With adaptation, the metabolic onset of liver failure in the HT1 pig can be a model of acute and acute-on-chronic liver failure for the investigation of advanced therapies, such as the cell therapy described herein.

We found that although hepatocytes demonstrated long-term survival within lymph nodes, after a period of engraftment in the lymph

Figure 5. Lentiviral Integration Profile in Lymph Node Versus Liver Hepatocytes

(A) Relative integration frequency in genomic elements (TU [transcription units]) for transplanted hepatocytes that remained in lymph nodes or migrated to the liver. (B) Relative integration frequency in CpG-rich promoter regions versus other areas of the genome for transplanted hepatocytes that remained in lymph nodes or migrated to the liver. (C) Relative integration frequency based on distance upstream and downstream of transcription start sites for transplanted hepatocytes that remained in lymph nodes or migrated to the liver. (D) Relative integration frequency in tumor-associated genes versus other areas of the genome for transplanted hepatocytes that remained in lymph nodes or migrated to the liver. (E) Lenti integration into the *Fah* locus. 99% of the clones found in the liver were clones of cells that were present in lymph nodes. (F) Scatter dot plot graphs showing reads per kilobase million (RPKM) values for liver-enriched lenti-disrupted genes and the reporter gene (NIS) in control liver, native liver, hepatized lymph node, and control lymph node. Data are mean ± SEM.

Table 1. Genes with Most Frequent Lentiviral (LV)-Fah Integration

Lymph Node Hepatocytes					Liver Hepatocytes					
TopGenes	Number of IntegrationSites	Percent of IntegrationSites	Numberof Reads	Percentof Reads	TopGenes	Number of IntegrationSites	Percent of IntegrationSites	Numberof Reads	Percentof Reads	Enrichment
GLRX2	26	0.40	338,309	25.57	MIR9799	18	0.41	5,479,826	56.29	5.00
MIR9799	14	0.21	148,852	11.25	NDUFV2	53	1.20	1,669,810	17.15	5.76
LNPK	53	0.81	146,239	11.05	IFRD1	45	1.02	952,259	9.78	5.81
PDCD10	81	1.24	129,982	9.82	SUCLG1	24	0.54	707,921	7.27	5.06
BEX1	51	0.78	41,620	3.15	CENPP	77	1.75	328,807	3.38	78.69
NDUFV2	25	0.38	39,429	2.98	GPX2	36	0.82	78,896	0.81	5.63
IDO1	5	0.08	30,360	2.29	CTDSP2	45	1.02	41,364	0.42	13.71
FAH	206	3.15	28,545	2.16	RAB28	19	0.43	23,253	0.24	6.03
IFRD1	31	0.47	22,270	1.68	QKI	7	0.16	16,777	0.17	5.44
BMP5	35	0.54	19,409	1.47	GSTO1	21	0.48	14,074	0.14	7.22
MTRF1	65	0.99	19,077	1.44	ENY2	30	0.68	12,470	0.13	3.97
SUCLG1	10	0.15	19,033	1.44	PRMT6	26	0.59	12,390	0.13	0.25
ADAMTS1	17	0.26	17,754	1.34	C1QTNF3	49	1.11	11,544	0.12	1.44
HSD17B3	35	0.54	16,484	1.25	RGS5	13	0.30	11,377	0.12	2.02
SLC9A2	8	0.12	14,970	1.13	MTRF1	36	0.82	10,972	0.11	0.08
ACVR2A	53	0.81	13,296	1.00	SNCAIP	5	0.11	10,252	0.11	0.81
KCNJ2	5	0.08	12,294	0.93	CTSV	5	0.11	9,865	0.10	5.34
CLDN22	32	0.49	12,073	0.91	FAH	135	3.06	9,650	0.10	0.05

Enrichment was calculated as the percent of reads in the liver population divided by the percent of reads in the lymph node population of hepatocytes by gene.

node, a subset migrates to the liver. This phenomenon was limited in previous mouse studies and could be related to the unique microanatomy and inverted direction of flow, unique to pig lymph nodes.[21] Their germinal centers are located internal to the medulla, which has suggested that lymphocytes are transported back into capillaries after passing through a lymph node, as opposed to into the lymphatic system as in other animals.[35,36] Indeed, during the injection procedure, it was possible to observe injected fluid communicating from the lymph node into the capillary bed. Interestingly, of the 135 unique *Fah* integration sites identified in the corrected hepatocytes engrafted in the liver, only one was not among the 206 unique integration sites observed in the lymph node hepatocytes. These data strongly indicate that the corrected cells in the liver are a subset of those found in the lymph nodes. Since these animals were weaned off NTBC after their transplantation procedure, it is possible that this earlier disease state was less receptive to treated cells. Once a therapeutic benefit was realized, the liver environment may have become more receptive to corrected cell engraftment. This hypothesis warrants further investigation to enhance efficacy of this procedure once translated to clinical applications.

In both liver and lymph node hepatocyte populations, the vector showed a benign integration profile with no preference for integration in promoter regions or tumor-associated genes. Prevalence of the top four integrated genes in the liver population was approximately five-fold higher than in the lymph node population, a linearity possibly supported by a single founder with all four integrations or up to 4 unique founders with identical (unbiased) expansion after migration to liver. Of note, *Fah* was within the top twenty genes with the highest integration frequency and was the gene with the highest number of distinct integration sites in both groups, suggesting a possible role for homology in vector integration. This should also be further explored to improve the safety of lentiviral genomic disruption.

In summary, we show that ectopic transplantation of corrected, autologous hepatocytes into mesenteric lymph nodes is curative in the HT1 pig model of liver failure. Hepatocyte transplantation into lymph nodes, which holds several important advantages over more traditional cell-transplantation techniques, especially in patients with pre-existing native liver damage, is a promising approach to the treatment of multiple liver diseases. Furthermore, this approach would not be clinically limited to autologous-corrected cells, as healthy allogeneic, universal donor, induced pluripotent stem cell (iPSC)-derived, and histocompatibility leukocyte antigen (HLA)-matched farmed hepatocytes could all be potential sources where partial hepatectomy may be contra-indicated.[37–39] Collectively, our data advocate for both the safety of the development of an ectopic liver in lymph nodes to treat liver failure and *ex vivo* gene therapy via lentiviral vectors. In addition to the clinical success of *ex vivo* lentiviral gene therapy in cancer and numerous hematologic disorders with over 250 open US Food and Drug Administration (FDA) trials,

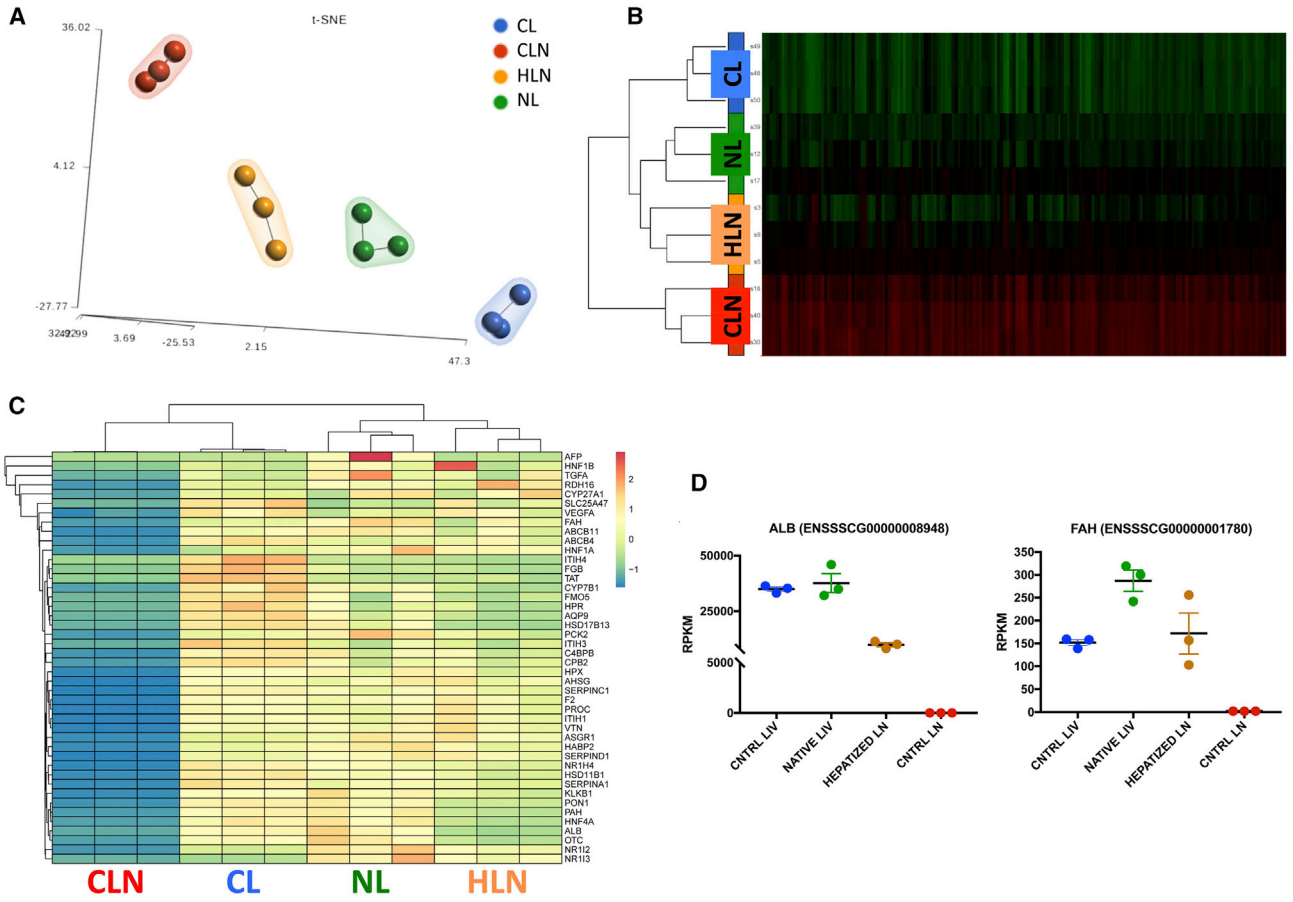

Figure 6. Transcriptional Identity of Hepatized Lymph Nodes (HLNs)

(A) t-Distributed Stochastic Neighbor Embedding (t-SNE) 2D plot of RNA-seq data, color-coded by tissue sample, showing evidence of HLN tendency to cluster with liver samples. CL, control liver (wild type); CLN, control lymph node (FAH knockout [KO]); NL, native liver (treated FAH KO). (B) Heatmap showing the normalized RNA-seq expression levels (reads per kilobase million [RPKM]) of differentially expressed genes across the four conditions. Red and green color intensity indicates gene upregulation and downregulation, respectively. (C) Heatmap showing the normalized RPKM of liver-specific differentially expressed genes across the four conditions. Spectral colors were used, with blue indicating low expression values, yellow indicating intermediately expressed genes, and red representing highly expressed genes. (D) RPKM values for *albumin* (ALB) and *Fah* in CL, NL, HLN, and CLN. Data are mean ± SEM.

making use of lentivirus, our data support progression of this paradigm into additional indications.[40] Ultimately, approval of expanded clinical applications of *ex vivo* lentiviral gene therapy will be made on a risk-reward basis, and a growing body of literature from our laboratory and others supports both safety (reduced risk) and efficacy (increased reward) of this approach.

MATERIALS AND METHODS

Animals

All animal procedures were performed in compliance with Mayo Clinic's Institutional Animal Care and Use Committee (IACUC) regulations, and all animals received humane care. This study evaluated wild-type and $Fah^{-/-}$ pigs that were 50% Large White and 50% Landrace lines.[33,41] NTBC was administered orally at 1 mg · kg^{-1} · day^{-1} (maximum of 25 mg/day) until transplantation, after which, NTBC was discontinued to support expansion of corrected cells. Animals were monitored daily and weighed regularly thereafter. NTBC treatment was reinitiated for 7 days, as needed, to support health.

Liver Resection and Hepatocyte Isolation

8-week-old (16–21 kg) pigs underwent a laparoscopic partial hepatectomy (15%–20% of total liver mass) involving the left lateral lobe under inhaled general anesthesia with 1%–3% isoflurane, as previously described.[42] The excised section was perfused to isolate hepatocytes, as previously described.[43]

Hepatocyte Radiolabeling

For biodistribution experiments, hepatocytes were radiolabeled in suspension with ^{89}Zr ($t_{1/2}$ = 78.4 h) with synthon ^{89}Zr-DBN at 27°C for 45 min in Hank's balanced salt solution (HBSS), as previously described.[44–46]

Hepatocyte Transduction

Hepatocytes were cotransduced in suspension at a MOI of 20 transcription units (TUs) with two, third-generation lentiviral vectors carrying the *Nis* reporter gene[47] or the pig *Fah* gene under control of the liver-specific pig TBG (Figure 1A). Transduction occurred for 2 h before resuspension in 0.9% sodium chloride (Baxter Healthcare, Deerfield, IL, USA) and transplantation as previously described.[10]

Hepatocyte Transplantation

All pigs received autologous transplantation of hepatocytes through direct mesenteric lymph node injection (Figure 1B). After partial hepatectomy, animals were kept under general anesthesia until the time of transplantation, approximately 4 h later. Bowel was exteriorized through the upper midline incision until the root of the mesentery was visible (Figure 1C). Hepatocytes were delivered directly into 10–20 mesenteric lymph nodes through direct injection with a 25G needle (Table S1). Each animal received a total of 6×10^8 hepatocytes in 10–20 mL of saline heparinization at 70 U/kg, as previously described for islet cell transplantation protocols.[48]

PET-CT

Imaging was performed on the high-resolution GE Discovery 690 ADC PET/CT System (GE Healthcare, Chicago, IL, USA) at scheduled times in the ^{89}Zr-labeled animal. Noninvasive evaluation of NIS expression was performed by PET/CT at scheduled times in two of the NIS-labeled animals using a [^{18}F]TFB radiotracer.[10] CT was performed at 120 kV and 150 mA, with tube rotation of 0.5 s and pitch of 0.516. PET was performed as a two-bed acquisition with 10 min per bed and 17 slice overlap, resulting in a 27-cm axial field of view. PMOD (version 3.711; PMOD Technologies, Switzerland) was used for image processing and analysis. Volumes of interest (VOIs) of mesenchymal lymph nodes were created on PET images, and SUVs for body weight were obtained.

Biochemical Analysis

Standard serum chemistry (including AST, ALP, total bilirubin, and ammonia) was performed using the Pioccolo Xpress Chemistry Analyzer (Abaxis, Union City, CA, USA) with a minimum sample size of 150 μL. Tyrosine values in plasma were determined using liquid chromatography and tandem mass spectrometry via Mayo Clinic's internal plasma amino acid analysis.

Histopathology and IHC

For H&E, Masson's trichrome, and FAH stains, tissue samples were fixed in 10% neutral-buffered formalin (Azer Scientific, Morgantown, PA, USA), paraffin embedded, and sectioned (5 μm). Standard stains were performed with established protocols, whereas IHC for Ki-67 was performed using monoclonal mouse anti-Ki-67 M7240 (Dako, Santa Clara, CA, USA), and FAH was performed as previously described.[47] Images were quantified in Aperio ImageScope. For all other IHC stains, tissues were fixed in 4% paraformaldehyde for 4 h, infiltrated with 30% sucrose overnight, and embedded in optimal cutting temperature (OCT) compound for sectioning (5–7 μm). Sections were washed with PBS, blocked with 5% bovine serum albumin (BSA) for 30 min, incubated with primary antibody for 1 h and secondary antibody for 30 min, and counterstained with Hoechst. Images were captured with an Olympus IX71 microscope. The following primary antibodies were used: ER-TR7 and glutamine synthetase cytokeratin 7 (ab51824, ab64613, ab9021; Abcam, Cambridge, MA, USA); CD31 (MCA1746GA; Bio-Rad, Hercules, CA, USA); cytokeratin 18 (ab668, Abcam, Cambridge, MA, USA); and 10830-1-AP, Proteintech, Chicago, IL, USA); and cytokeratin 19 (ab84632; Abcam, Cambridge, MA, USA).

Mapping of Lentiviral Integration Sites

Genomic DNA was isolated from snap-frozen tissue fragments of hepatized mesenteric lymph nodes and engrafted livers from animal number 265 using a Gentra Puregene Tissue Kit (QIAGEN, Hilden, Germany). Ligation-mediated PCR (LM-PCR) was used for isolation of integration sites. Genomic DNA was restricted with MseI, ligated to linkers, and treated with ApoI to limit amplification of vector fragments. Samples were amplified by nested PCR and sequenced using the Illumina HiSeq 2500 Next-Generation Sequencing System (San Diego, CA). Presence of both viral and genomic sequence verified reads that reported an integration. Picard software (http://broadinstitute.github.io/picard/) calculated the average fragment length per sample. Averaged sequence length was 158 ± 29 bp. Reads were trimmed to remove (1) viral sequence using cutadapt[49] and (2) any linker sequence. Trimmed reads less than 15 bp and untrimmed reads were removed from analysis since they could not be reliably mapped. Remaining reads were aligned to the susScr11 build of the pig reference genome using default parameters of burrows-wheeler aligner (BWA)-MEM in single-end mode.[50] Integration points were defined by the position of the first aligned genomic base with ≥ 5 supporting reads.

Locations of integration points were categorized in the following: exons, introns, 3′ UTRs, 5′ UTRs, and intergenic regions using information extracted from the susScr11 refFlat file maintained by the University of California Santa Cruz's (UCSC's) Genomics Institute using the longest gene to annotate integrations. Distance to transcription start site (TSS), makeup of CpG-rich regions of the genome ("CpG islands"), and enrichment to a list of 745 tumor-associated genes (Mayo Clinic internal) were computed.

Whole Transcriptome RNA Sequencing (RNA-Seq)

Total RNA was isolated from snap-frozen samples of liver and mesenteric lymph nodes using the RNeasy Mini Kit (QIAGEN, Valencia, CA, USA), according to the manufacturer's instructions. RNA was measured using a NanoDrop 2000/c spectrophotometer (Thermo Fisher Scientific, Pittsburgh, PA, USA). Screening of HLNs was performed by examining *albumin* and *fah* expression using quantitative reverse transcriptase PCR (qRT-PCR). Nontransplanted mesenteric lymph nodes and CL were used as negative and positive controls, respectively. RNA was retrotranscribed using the iScript Reverse Transcription Supermix (Bio-Rad, Hercules, CA, USA), and *albumin* and *fah* were amplified using the SsoAdvanced Universal SYBR Green Supermix (Bio-Rad, Hercules, CA, USA) on a StepOnePlus

System (Applied Biosystems, Foster City, CA, USA). Expression of glyceraldehyde-3-phosphate dehydrogenase (GAPDH) was used for expression normalization. Selected RNAs were shipped on dry ice to Novogene (Sacramento, CA, USA) for library preparation and sequencing. Analysis was performed using Partek Genomics Suite software v.7.0. Transcript abundance was estimated by an expectation-maximization algorithm and expressed as FPKM (fragments per kilobase million). DE genes were detected using differential gene-expression (Gene-Set Analysis [GSA]) algorithm. 12,000 genes were identified as DE based on log2 |fold change (FC)| $\geq$ 2 and false discovery rate (FDR) $\geq$ 0.05 cutoff. Unsupervised clustering to visualize expression signature was performed using 1-Pearson correlation distance and complete linkage rule, and samples were classified using t-SNE.

Statistical Analysis

Numerical data are mean ± SD (standard deviation) or SEM (standard error of the mean). Statistical significance was determined by Welch's t test at $p \leq 0.05$ using GraphPad Prism software version 7.

SUPPLEMENTAL INFORMATION

Supplemental Information can be found online at https://doi.org/10.1016/j.omtm.2020.07.009.

AUTHOR CONTRIBUTIONS

C.T.N., R.A.K., and J.B.L. designed and performed experiments and wrote the manuscript. R.D.H., E.L., S.L.N., and J.B.L. conceived and interpreted the study. K.L.A., C.J.V., R.M.G., B.A., L.S., B.H., M.G.F., A.C., H.J., A.B., M.K.P., I.G., V.L., and T.R.G. provided scientific input and expertise to the execution and interpretation of results. A.B., D.O., and J.-P.A.K. performed the bioinformatics analysis and provided expertise. R.D.H., E.L., and J.-P.A.K. also reviewed the manuscript.

CONFLICTS OF INTEREST

E.L. is chief scientific officer of LyGenesis. J.B.L. and R.A.K. are officers of Cytotheryx. K.L.A. is an employee of Cytotheryx. R.D.H. is an employee of Ambys Medicines. All other authors declare no competing interests.

ACKNOWLEDGMENTS

We thank T. Wyman and L. Filzen for large-animal PET imaging support; L. Gross and L. Acosta for histology support; S. Krage and J. Pederson for surgical support; L. Hillin for animal support; and P. Steiner for graphical support. Funding for the project was received from NIH (K01 DK106056); Mayo CTSA (grant UL1TR000135); Regenerative Medicine Minnesota (RMM 101617TR002); Children's Minnesota Foundation; NIH (R01 DK114282 to B.H. and E.L.); Commonwealth of Pennsylvania (SAP4100073573 to M.G.F. and E.L.); and Ri.MED Foundation (to M.G.F.).

REFERENCES

1. Shafran, D., Kodish, E., and Tzakis, A. (2014). Organ shortage: the greatest challenge facing transplant medicine. World J. Surg. *38*, 1650–1657.
2. Soltys, K.A., Setoyama, K., Tafaleng, E.N., Soto Gutiérrez, A., Fong, J., Fukumitsu, K., Nishikawa, T., Nagaya, M., Sada, R., Haberman, K., et al. (2017). Host conditioning and rejection monitoring in hepatocyte transplantation in humans. J. Hepatol. *66*, 987–1000.
3. Schuppan, D., and Afdhal, N.H. (2008). Liver cirrhosis. Lancet *371*, 838–851.
4. Lindblad, B., Lindstedt, S., and Steen, G. (1977). On the enzymic defects in hereditary tyrosinemia. Proc. Natl. Acad. Sci. USA *74*, 4641–4645.
5. Bartlett, D.C., Lloyd, C., McKiernan, P.J., and Newsome, P.N. (2014). Early nitisinone treatment reduces the need for liver transplantation in children with tyrosinaemia type 1 and improves post-transplant renal function. J. Inherit. Metab. Dis. *37*, 745–752.
6. Grompe, M. (2001). The pathophysiology and treatment of hereditary tyrosinemia type 1. Semin. Liver Dis. *21*, 563–571.
7. Endo, F., and Sun, M.S. (2002). Tyrosinaemia type I and apoptosis of hepatocytes and renal tubular cells. J. Inherit. Metab. Dis. *25*, 227–234.
8. Lindstedt, S., Holme, E., Lock, E.A., Hjalmarson, O., and Strandvik, B. (1992). Treatment of hereditary tyrosinaemia type I by inhibition of 4-hydroxyphenylpyruvate dioxygenase. Lancet *340*, 813–817.
9. Elgilani, F., Mao, S.A., Glorioso, J.M., Yin, M., Iankov, I.D., Singh, A., Amiot, B., Rinaldo, P., Marler, R.J., Ehman, R.L., et al. (2017). Chronic Phenotype Characterization of a Large-Animal Model of Hereditary Tyrosinemia Type 1. Am. J. Pathol. *187*, 33–41.
10. Hickey, R.D., Mao, S.A., Glorioso, J., Elgilani, F., Amiot, B., Chen, H., Rinaldo, P., Marler, R., Jiang, H., DeGrado, T.R., et al. (2016). Curative ex vivo liver-directed gene therapy in a pig model of hereditary tyrosinemia type 1. Sci. Transl. Med. *8*, 349ra99.
11. Hughes, R.D., Mitry, R.R., and Dhawan, A. (2012). Current status of hepatocyte transplantation. Transplantation *93*, 342–347.
12. von Andrian, U.H., and Mempel, T.R. (2003). Homing and cellular traffic in lymph nodes. Nat. Rev. Immunol. *3*, 867–878.
13. Junt, T., Scandella, E., and Ludewig, B. (2008). Form follows function: lymphoid tissue microarchitecture in antimicrobial immune defence. Nat. Rev. Immunol. *8*, 764–775.
14. Sleeman, J.P., and Thiele, W. (2009). Tumor metastasis and the lymphatic vasculature. Int. J. Cancer *125*, 2747–2756.
15. Saharinen, P., Tammela, T., Karkkainen, M.J., and Alitalo, K. (2004). Lymphatic vasculature: development, molecular regulation and role in tumor metastasis and inflammation. Trends Immunol. *25*, 387–395.
16. Tammela, T., and Alitalo, K. (2010). Lymphangiogenesis: Molecular mechanisms and future promise. Cell *140*, 460–476.
17. Link, A., Vogt, T.K., Favre, S., Britschgi, M.R., Acha-Orbea, H., Hinz, B., Cyster, J.G., and Luther, S.A. (2007). Fibroblastic reticular cells in lymph nodes regulate the homeostasis of naive T cells. Nat. Immunol. *8*, 1255–1265.
18. Fletcher, A.L., Acton, S.E., and Knoblich, K. (2015). Lymph node fibroblastic reticular cells in health and disease. Nat. Rev. Immunol. *15*, 350–361.
19. DeWard, A.D., Komori, J., and Lagasse, E. (2014). Ectopic transplantation sites for cell-based therapy. Curr. Opin. Organ Transplant. *19*, 169–174.
20. Hoppo, T., Komori, J., Manohar, R., Stolz, D.B., and Lagasse, E. (2011). Rescue of lethal hepatic failure by hepatized lymph nodes in mice. Gastroenterology *140*, 656–666.e2.
21. Komori, J., Boone, L., DeWard, A., Hoppo, T., and Lagasse, E. (2012). The mouse lymph node as an ectopic transplantation site for multiple tissues. Nat. Biotechnol. *30*, 976–983.
22. Zhang, Y., Hong, H., and Cai, W. (2011). PET tracers based on Zirconium-89. Curr. Radiopharm. *4*, 131–139.
23. Cardoso, L.M.D.F., Moreira, L.F.P., Pinto, M.A., Henriques-Pons, A., and Alves, L.A. (2018). Domino Hepatocyte Transplantation: A Therapeutic Alternative for the Treatment of Acute Liver Failure. Can. J. Gastroenterol. Hepatol. *2018*, 2593745.
24. Gebhardt, R., Baldysiak-Figiel, A., Krügel, V., Ueberham, E., and Gaunitz, F. (2007). Hepatocellular expression of glutamine synthetase: an indicator of morphogen

actions as master regulators of zonation in adult liver. Prog. Histochem. Cytochem. *41*, 201–266.

25. Dhawan, A., Strom, S.C., Sokal, E., and Fox, I.J. (2010). Human hepatocyte transplantation. Methods Mol. Biol. *640*, 525–534.
26. Habibullah, C.M., Syed, I.H., Qamar, A., and Taher-Uz, Z. (1994). Human fetal hepatocyte transplantation in patients with fulminant hepatic failure. Transplantation *58*, 951–952.
27. Kobayashi, N., Ito, M., Nakamura, J., Cai, J., Gao, C., Hammel, J.M., and Fox, I.J. (2000). Hepatocyte transplantation in rats with decompensated cirrhosis. Hepatology *31*, 851–857.
28. Thornburg, B., Desai, K., Hickey, R., Kulik, L., Ganger, D., Baker, T., Abecassis, M., Lewandowski, R.J., and Salem, R. (2016). Portal Vein Recanalization and Transjugular Intrahepatic Portosystemic Shunt Creation for Chronic Portal Vein Thrombosis: Technical Considerations. Tech. Vasc. Interv. Radiol. *19*, 52–60.
29. Francipane, M.G., Han, B., Oxburgh, L., Sims-Lucas, S., Li, Z., and Lagasse, E. (2019). Kidney-in-a-lymph node: A novel organogenesis assay to model human renal development and test nephron progenitor cell fates. J. Tissue Eng. Regen. Med. *13*, 1724–1731.
30. Francipane, M.G., and Lagasse, E. (2016). Regenerating a kidney in a lymph node. Pediatr. Nephrol. *31*, 1553–1560.
31. Francipane, M.G., and Lagasse, E. (2016). Pluripotent Stem Cells to Rebuild a Kidney: The Lymph Node as a Possible Developmental Niche. Cell Transplant. *25*, 1007–1023.
32. Senti, G., Prinz Vavricka, B.M., Erdmann, I., Diaz, M.I., Markus, R., McCormack, S.J., Simard, J.J., Wüthrich, B., Crameri, R., Graf, N., et al. (2008). Intralymphatic allergen administration renders specific immunotherapy faster and safer: a randomized controlled trial. Proc. Natl. Acad. Sci. USA *105*, 17908–17912.
33. Hickey, R.D., Mao, S.A., Glorioso, J., Lillegard, J.B., Fisher, J.E., Amiot, B., Rinaldo, P., Harding, C.O., Marler, R., Finegold, M.J., et al. (2014). Fumarylacetoacetate hydrolase deficient pigs are a novel large animal model of metabolic liver disease. Stem Cell Res. (Amst.) *13*, 144–153.
34. Dhawan, A., Puppi, J., Hughes, R.D., and Mitry, R.R. (2010). Human hepatocyte transplantation: current experience and future challenges. Nat. Rev. Gastroenterol. Hepatol. *7*, 288–298.
35. Hunt, A.C. (1968). Micro-anatomy of the lymph nodes of the pig. Br. J. Exp. Pathol. *49*, 338–339.
36. McFarlin, D.E., and Binns, R.M. (1973). Lymph node function and lymphocyte circulation in the pig. Adv. Exp. Med. Biol. *29*, 87–93.
37. Mattapally, S., Pawlik, K.M., Fast, V.G., Zumaquero, E., Lund, F.E., Randall, T.D., Townes, T.M., and Zhang, J. (2018). Human Leukocyte Antigen Class I and II Knockout Human Induced Pluripotent Stem Cell-Derived Cells: Universal Donor for Cell Therapy. J. Am. Heart Assoc. *7*, e010239.
38. Takebe, T., Zhang, R.R., Koike, H., Kimura, M., Yoshizawa, E., Enomura, M., Koike, N., Sekine, K., and Taniguchi, H. (2014). Generation of a vascularized and functional human liver from an iPSC-derived organ bud transplant. Nat. Protoc. *9*, 396–409.
39. Grompe, M., and Strom, S. (2013). Mice with human livers. Gastroenterology *145*, 1209–1214.
40. Milone, M.C., and O'Doherty, U. (2018). Clinical use of lentiviral vectors. Leukemia *32*, 1529–1541.
41. Hickey, R.D., Lillegard, J.B., Fisher, J.E., McKenzie, T.J., Hofherr, S.E., Finegold, M.J., Nyberg, S.L., and Grompe, M. (2011). Efficient production of Fah-null heterozygote pigs by chimeric adeno-associated virus-mediated gene knockout and somatic cell nuclear transfer. Hepatology *54*, 1351–1359.
42. Kaiser, R.A., Mao, S.A., Glorioso, J., Amiot, B., Nicolas, C.T., Allen, K.L., Du, Z., VanLith, C.J., Hickey, R.D., Nyberg, S.L., and Lillegard, J.B. (2018). Lentiviral Vector-mediated Gene Therapy of Hepatocytes Ex Vivo for Autologous Transplantation in Swine. J. Vis. Exp. (141), e58399.
43. Sielaff, T.D., Hu, M.Y., Rao, S., Groehler, K., Olson, D., Mann, H.J., Remmel, R.P., Shatford, R.A., Amiot, B., Hu, W.S., et al. (1995). A technique for porcine hepatocyte harvest and description of differentiated metabolic functions in static culture. Transplantation *59*, 1459–1463.
44. Pandey, M.K., Bansal, A., Engelbrecht, H.P., Byrne, J.F., Packard, A.B., and DeGrado, T.R. (2016). Improved production and processing of ^{89}Zr using a solution target. Nucl. Med. Biol. *43*, 97–100.
45. Pandey, M.K., Engelbrecht, H.P., Byrne, J.P., Packard, A.B., and DeGrado, T.R. (2014). Production of 89Zr via the 89Y(p,n)89Zr reaction in aqueous solution: effect of solution composition on in-target chemistry. Nucl. Med. Biol. *41*, 309–316.
46. Bansal, A., Pandey, M.K., Demirhan, Y.E., Nesbitt, J.J., Crespo-Diaz, R.J., Terzic, A., Behfar, A., and DeGrado, T.R. (2015). Novel (89)Zr cell labeling approach for PET-based cell trafficking studies. EJNMMI Res. *5*, 19.
47. Hickey, R.D., Mao, S.A., Amiot, B., Suksanpaisan, L., Miller, A., Nace, R., Glorioso, J., O'Connor, M.K., Peng, K.W., Ikeda, Y., et al. (2015). Noninvasive 3-dimensional imaging of liver regeneration in a mouse model of hereditary tyrosinemia type 1 using the sodium iodide symporter gene. Liver Transpl. *21*, 442–453.
48. Shapiro, A.M. (2012). Islet transplantation in type 1 diabetes: ongoing challenges, refined procedures, and long-term outcome. Rev. Diabet. Stud. *9*, 385–406.
49. Martin, M. (2011). Cutadapt removes adapter sequences from high-throughput sequencing reads. EMBnet.journal *17*, 10–12.
50. Li, H., and Durbin, R. (2009). Fast and accurate short read alignment with Burrows-Wheeler transform. Bioinformatics *25*, 1754–1760.

OMTM, Volume *18*

Supplemental Information

Ex Vivo Cell Therapy by Ectopic Hepatocyte Transplantation Treats the Porcine Tyrosinemia Model of Acute Liver Failure

Clara T. Nicolas, Robert A. Kaiser, Raymond D. Hickey, Kari L. Allen, Zeji Du, Caitlin J. VanLith, Rebekah M. Guthman, Bruce Amiot, Lukkana Suksanpaisan, Bing Han, Maria Giovanna Francipane, Amin Cheikhi, Huailei Jiang, Aditya Bansal, Mukesh K. Pandey, Ishan Garg, Val Lowe, Aditya Bhagwate, Daniel O'Brien, Jean-Pierre A. Kocher, Timothy R. DeGrado, Scott L. Nyberg, Eric Lagasse, and Joseph B. Lillegard

Supplementary Materials

Supplementary Table 1. Summary of cell transplantations.

Pig ID	Sex	Weight at Transplant (kg)	Live Cells Harvested (x 10^6)	Viability (%)	Injection Volume of Saline (mL)	Number of Lymph Nodes Injected	Cells Transplanted (x 10^6)	Cells Transplanted (x 10^6/kg)	Days of Follow-up
265	Female	20.8	1160	84	10	10-20	600	28.8	239
268	Male	19.8	770	77	20	10-20	600	30.3	235
270	Male	16.4	995	82	20	10-20	600	36.6	241
272	Male	19.0	975	74	20	10-20	600	31.6	212
278	Female	19.6	671	85	20	10-20	600	30.6	239

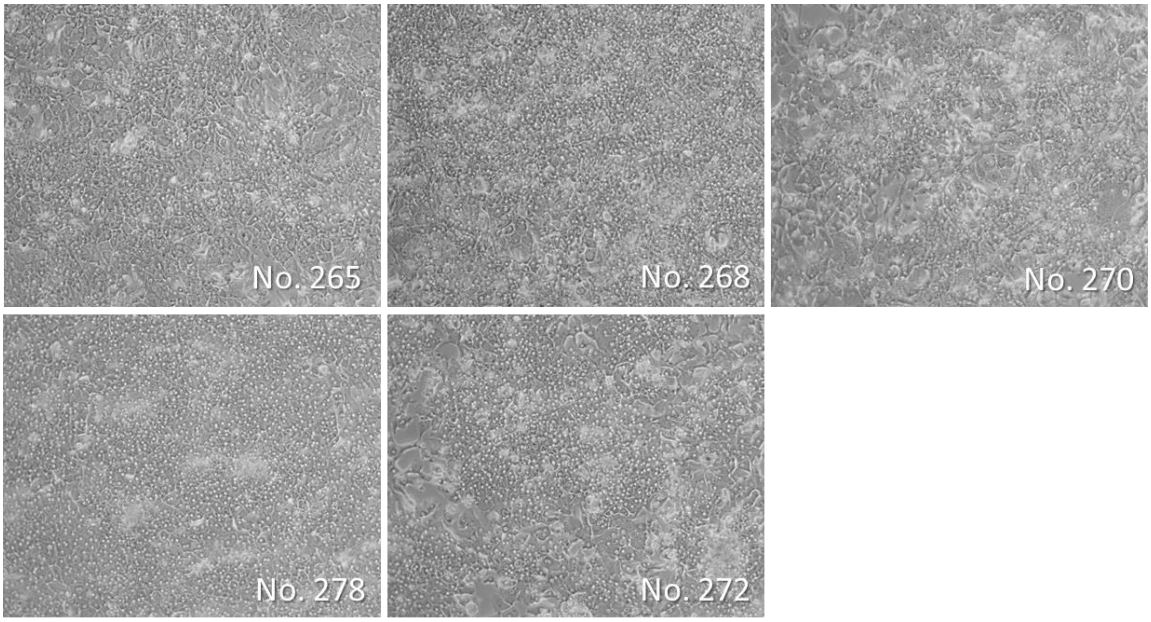

Supplementary Figure 1. Isolated hepatocytes for autotransplantaton were platable in culture. Representative hepatocytes from all pigs (Nos. 265, 268, 270, 278, and 272) were cultured for a full 48 hours after isolation to evaluative platability, which was qualitatively evaluated as a surrogate indicator for predicting engraftment *in vivo*.

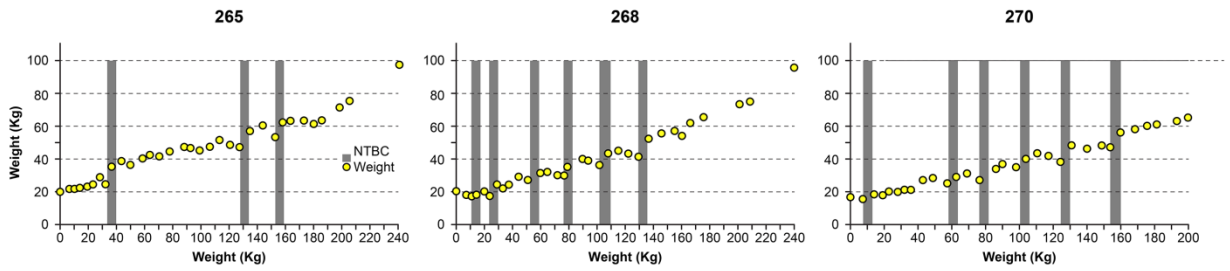

Supplementary Figure 2. Weight stabilization of pigs 265, 268, and 270. NTBC-independent weight gain was achieved at days 158, 133, and 163, respectively, after three to six cycles on the drug (represented by gray vertical bars).

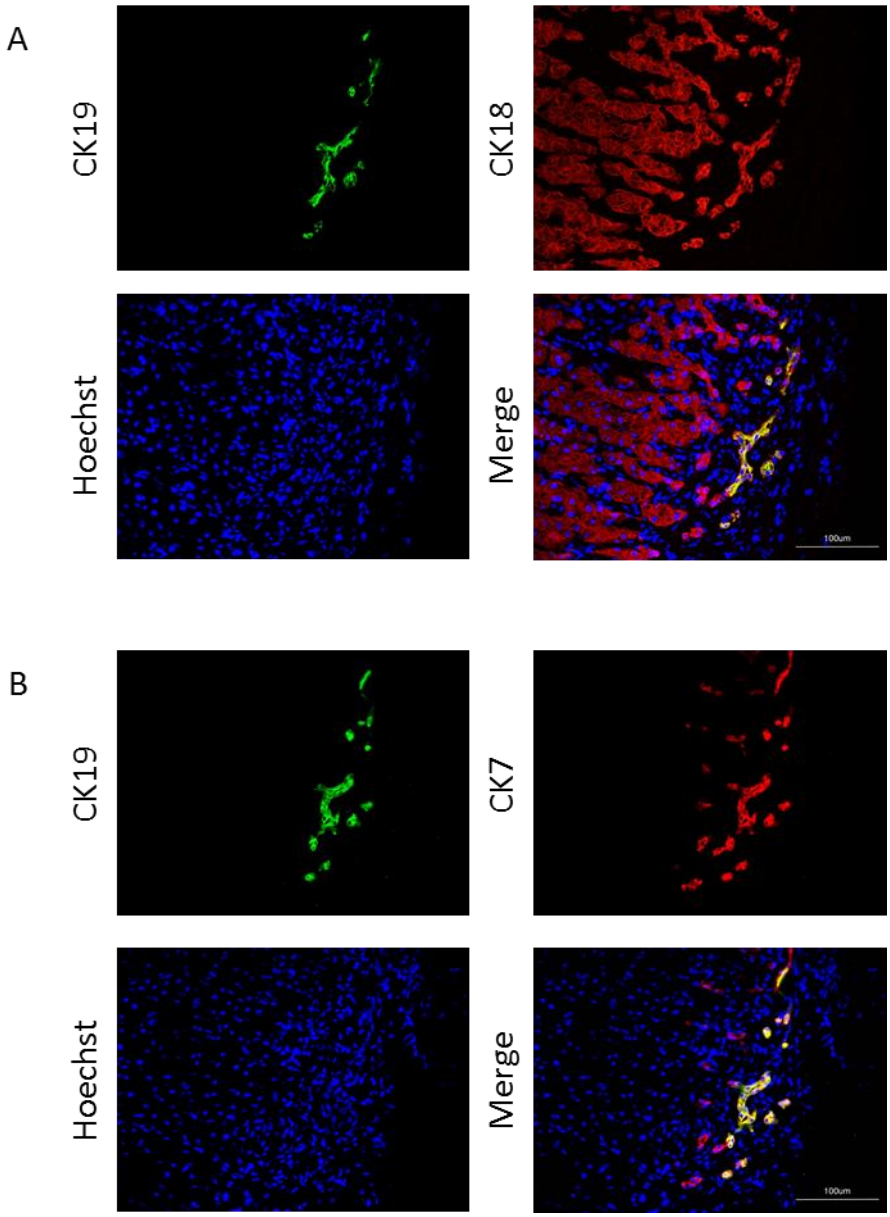

Supplementary Figure 3. Regions of hepatocyte engraftment in lymph nodes develop bile duct cells. Bile duct cell presence was further explored in Pig No. 265. A) At the periphery of nodules of hepatocyte engraftment and expansion, rare sections also contain cells that express CK19 (green), a common marker for bile duct cells. CK18 (red) and Hoechst staining demonstrate the presence of the hepatocytes in this section, verifying that it is a site of engraftment. B) All CK19-positive cells (green) were also positive for CK7 (red), although the

merged panel indicates that only the majority of CK7 positive cells were also positive for CK19 (co-localization in yellow).

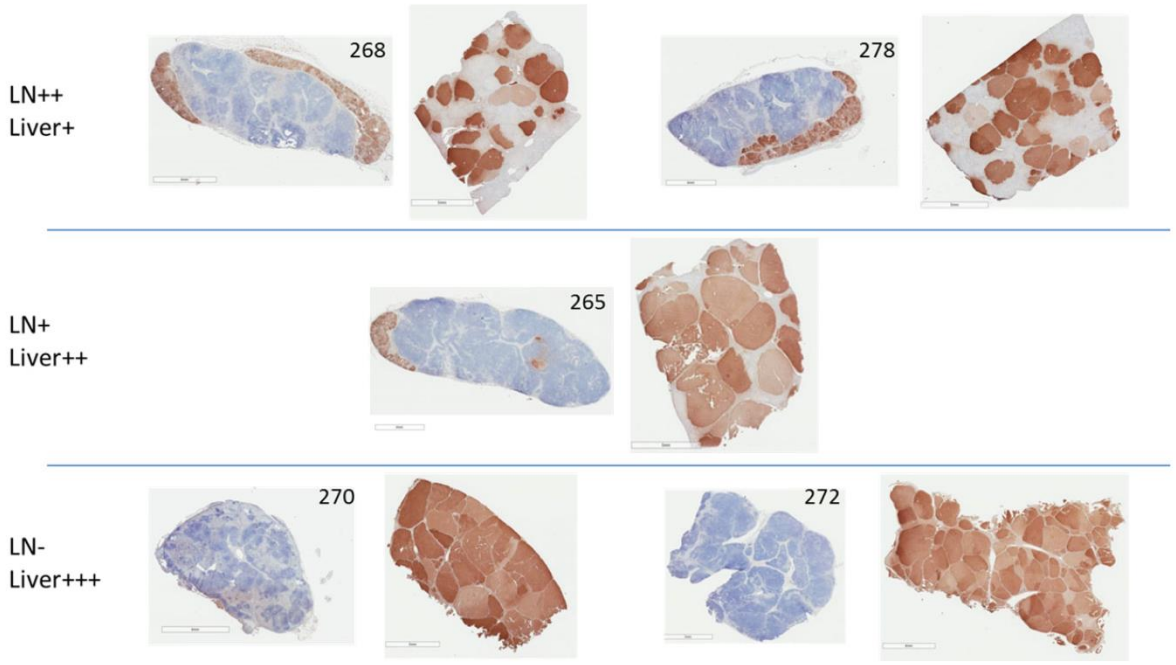

Supplementary Figure 4. Correlation between presence of FAH-positive hepatocytes in lymph node and liver. Animals with partial liver repopulation with FAH-positive hepatocytes (pigs 268 and 278) still had robust ectopic liver tissue presence in lymph nodes at the time of euthanization. Animals with complete liver repopulation with FAH-positive hepatocytes (pigs 270 and 272) had little to no presence of ectopic liver tissue in lymph nodes at the time of euthanization.

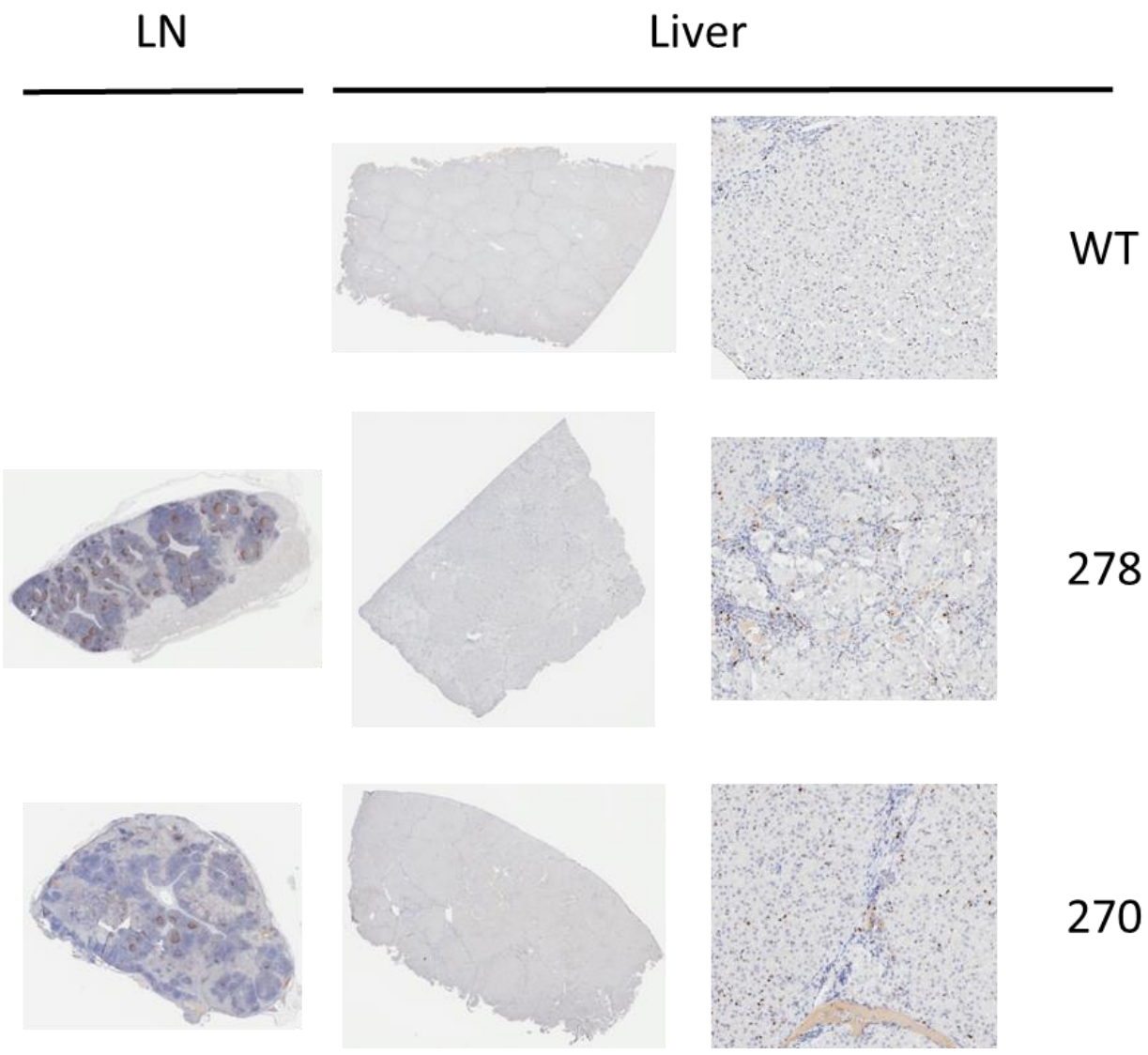

Supplementary Figure 5. Eight months after transplantation, hepatocytes in lymph nodes and livers are not actively proliferating. At termination (approximately 8 months post-transplantation) animals with partial liver repopulation with FAH-positive hepatocytes (such as pig 268) and those with complete liver repopulation with FAH-positive hepatocytes (such as pig 270) showed unremarkable Ki-67 positivity relative to wild type pig liver (top row), indicating that proliferation in both tissues was largely complete at the time of termination.

Supplementary Table 2. Next generation sequencing mapping statistics

Sample	Total Reads	Mapped Reads (Total)	Integration Points at 1X	Integration Points at 5X
Lymph node	115.748.080	5,465,009 (7.34 %)	40.239	6.335
Liver	116.490.845	21,126,444 (22.29 %)	27.987	4.270

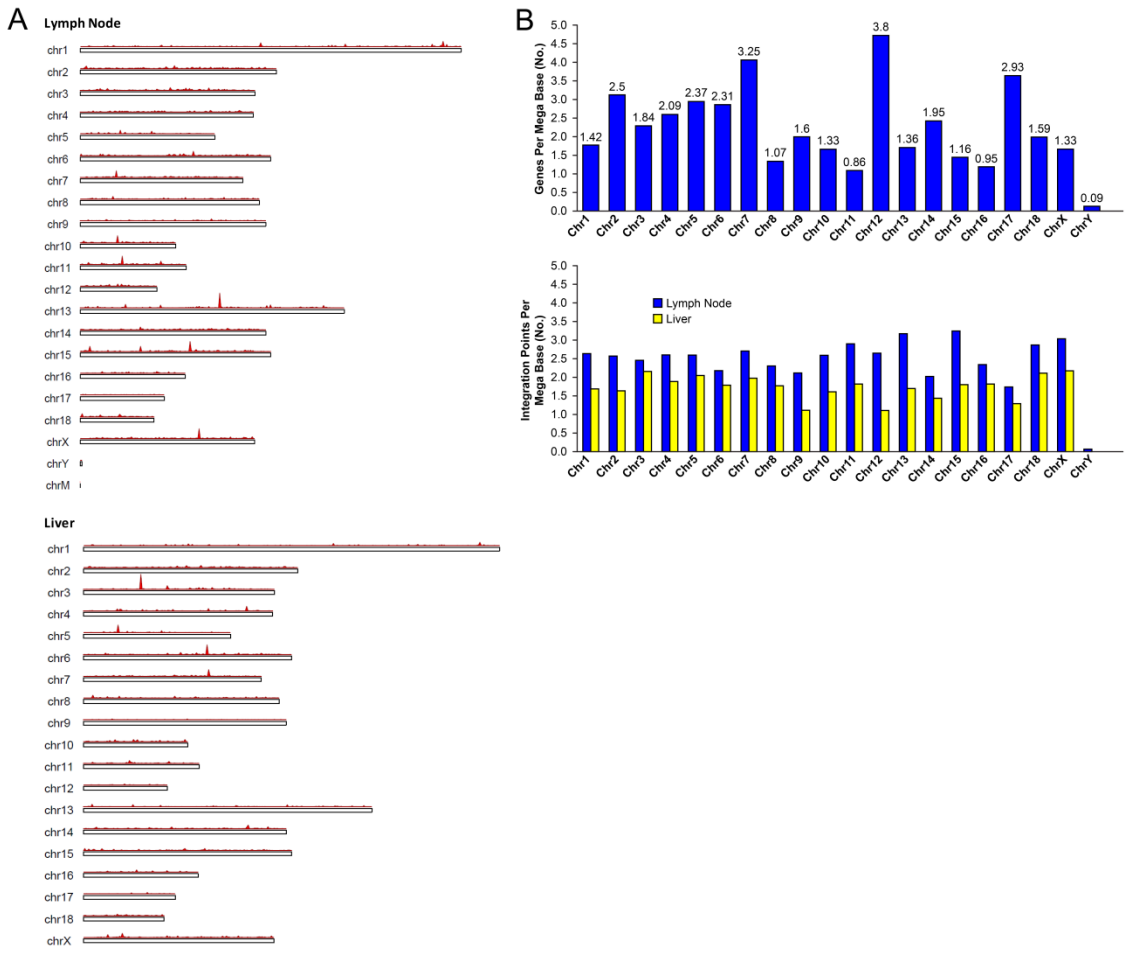

Supplementary Figure 6. Lentiviral integration profile in lymph node vs. liver hepatocytes. (A) Chromosomal integration map for transplanted hepatocytes that remained in lymph nodes (top) and transplanted hepatocytes that migrated to the liver (bottom). Red vertical bars represent integration points. (B) Relative gene density per chromosome (top) compared to relative integration density per chromosome (bottom).

Supplementary Table 3. Liver-specific genes included in RNA sequencing analysis

LiGEP		
ENSSSCG00000011799	AHSG	Alpha 2-HS glycoprotein
ENSSSCG00000008948	ALB	Albumin
ENSSSCG00000004597	AQP9	Aquaporin 9
ENSSSCG00000015661	C4BPB	C4b-binding protein beta chain
ENSSSCG00000009413	CPB2	Carboxypeptidase B2
ENSSSCG00000013252	F2	Coagulation factor II (thrombin)
ENSSSCG00000008997	FGB	Fibrinogen beta chain
ENSSSCG00000006702	FMO5	Flavin containing monooxygenase 5
ENSSSCG00000010639	HABP2	Hyaluronan binding protein 2
ENSSSCG00000002749	HPR	Haptoglobin
ENSSSCG00000014626	HPX	Hemopexin
ENSSSCG00000015616	HSD11B1	Hydroxysteroid (11-beta) dehydrogenase 1
ENSSSCG00000009225	HDD17B13	Hydroxysteroid (17-beta) dehydrogenase 13
ENSSSCG00000011450	ITIH1	Inter-alpha-trypsin inhibitor heavy chain H1
ENSSSCG00000011451	ITIH3	Inter-alpha-trypsin inhibitor heavy chain H3
ENSSSCG00000011453	ITIH4	Inter-alpha-trypsin inhibitor heavy chain H4
ENSSSCG00000015799	KLKB1	Plasma kallikrein
ENSSSCG00000015332	PON1	Paraoxonase 1
ENSSSCG00000023693	PROC	Vitamin K-dependent protein C
ENSSSCG00000000419	RDH16	Retinol dehydrogenase 16
ENSSSCG00000015493	SERPINC1	Antithrombin-III
ENSSSCG00000010093	SERPIND1	Heparin cofactor 2
ENSSSCG00000002515	SLC25A47	Solute carrier family 25 member 47
ENSSSCG00000027801	VTN	Vitronectin
Additional Liver-Specific Genes		
ENSSSCG00000016199	CYP27A1	Cytochrome P450 family 27 subfamily A member 1
ENSSSCG00000022092	CYP7B1	Cytochrome P450 family 7 subfamily B member 1
ENSSSCG00000001780	FAH	Fumarylacetoacetate hydrolase
ENSSSCG00000012236	OTC	Ornithine transcarbamylase
ENSSSCG00000000856	PAH	Phenylalanine hydroxylase
ENSSSCG00000002009	PCK2	Phosphoenolpyruvate carboxykinase 2
ENSSSCG00000002476	SERPINA1	Alpha-1-antitrypsin
ENSSSCG00000002736	TAT	Tyrosine aminotransferase
ENSSSCG00000008949	AFP	Alpha-fetoprotein
ENSSSCG00000024520	ABCB4	Adenosine triphosphate-binding cassette, subfamily B, member 4
ENSSSCG00000015926	ABCB11	Adenosine triphosphate–binding cassette B11
ENSSSCG00000009919	HNF1A	Hepatocyte nuclear factor 1 homeobox A
ENSSSCG00000022417	HNF1B	Hepatocyte nuclear factor-1-beta
ENSSSCG00000007371	HNF4A	Hepatocyte nuclear factor 4 alpha
ENSSSCG00000000875	NR1H4	Nuclear receptor subfamily 1 group H member 4
ENSSSCG00000011890	NR1I2	Nuclear receptor subfamily 1 group I member 2
ENSSSCG00000006353	NR1I3	Nuclear receptor subfamily 1 group I member 3
ENSSSCG00000024926	ASGR1	Asialoglycoprotein receptor 1
ENSSSCG00000008326	TGFA	Transforming growth factor alpha
ENSSSCG00000001695	VEGFA	Vascular endothelial growth factor A

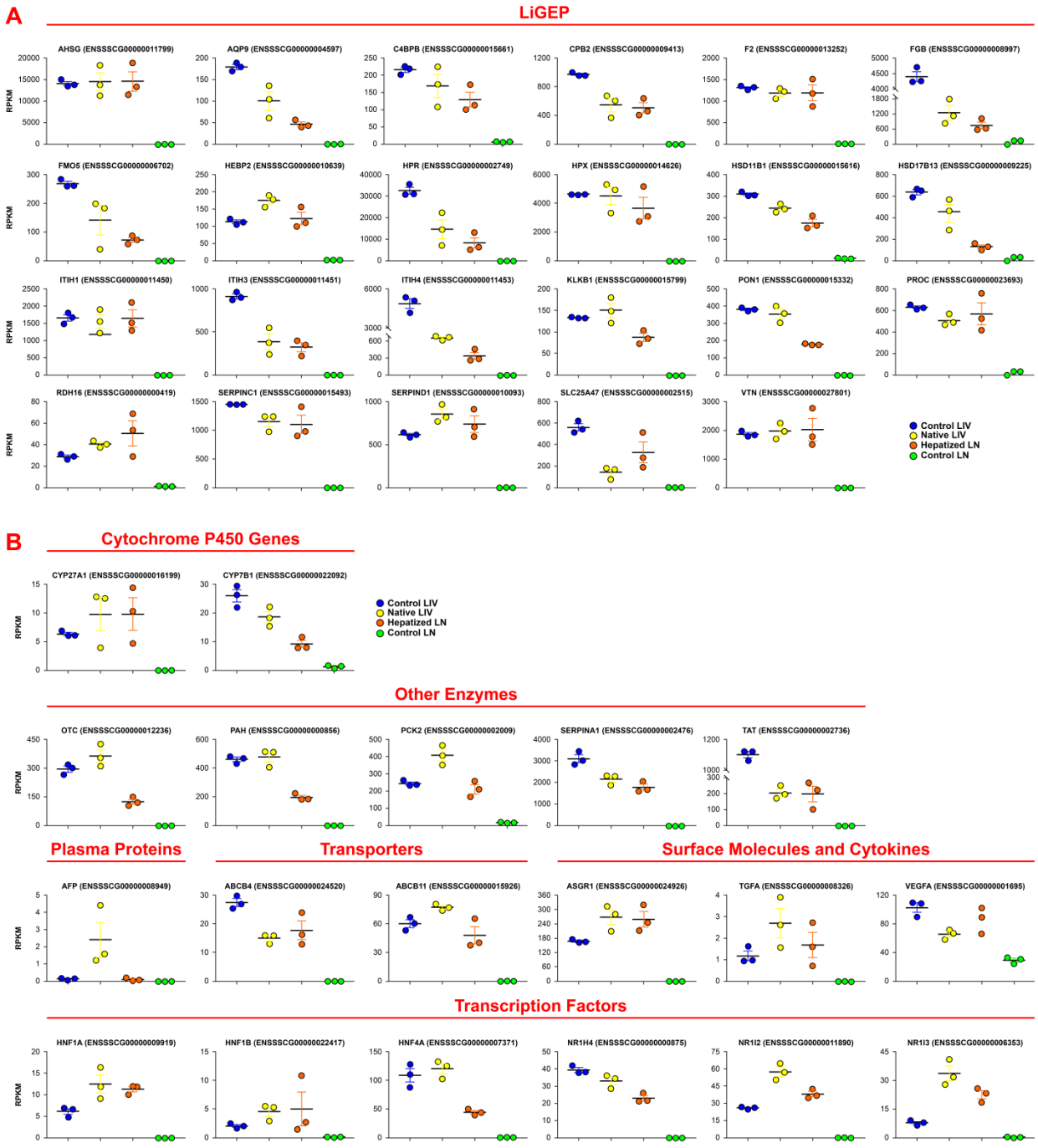

Supplementary Figure 7. Further RNA sequencing analysis. Scatter dot plot graphs showing RPKM values for LiGEP (liver-specific gene expression panel) (A) or additional liver-specific genes (B) in control liver, native liver, hepatized lymph node, and control lymph node. Data are mean ± SEM.

Supplementary Video 1. 3D render movie of PET-CT images of ^{89}Zr-labeled hepatocytes at 6 h post-transplantation into mesenteric lymph nodes in pig.

Supplementary Video 2. 3D render movie of PET-CT images of NIS-labeled hepatocytes at 3 months post-transplantation into mesenteric lymph nodes in pig 265.

Supplementary Video 3. 3D render movie of PET-CT images of NIS-labeled hepatocytes at 6 months post-transplantation into mesenteric lymph nodes in pig 265.

Supplementary Video 4. 3D render movie of PET-CT images of NIS-labeled hepatocytes at 5 months post-transplantation into mesenteric lymph nodes in pig 268.

Supplementary Video 5. 3D render movie of PET-CT images of NIS-labeled hepatocytes at 6 months post-transplantation into mesenteric lymph nodes in pig 268.